3D Full-Maxwell Simulations of Very Fast Transients in GIS

Jasmin Smajic[1], Walter Holaus[2], Jadran Kostovic[2], and Uwe Riechert[2]

[1]ABB Corporate Research Ltd., CH-5405 Segelhofstrasse 1K, Baden-Dättwil, Switzerland
[2]ABB Switzerland Ltd., CH-8050 Brown-Boveri-Strasse 5, Zurich, Switzerland

This study presents a detailed analysis of very fast electromagnetic transients (VFTs) initiated by disconnector switching operations in gas insulated switchgears (GIS). The results of the full-Maxwell electromagnetic simulations performed on real-life GIS geometries along with the modeling details are presented. The verification of the simulation results was performed by comparison against both measurements and circuit-equations-based transient simulations with the aim to quantify the achieved simulations' accuracy. The obtained results show a highly accurate shape and acceptably accurate amplitude prediction of dominant VFT waves in GIS, allowing for better understanding of the VFT phenomenon and a significant reduction of the product development time and prototyping costs.

***Index Terms*—Electromagntic (EM) transient propagation, full-Maxwell wave analysis, gas insulated switchgear (GIS), very fast transients (VFTs).**

I. Introduction

GIS are core high voltage (HV) components of electric power distribution and transmission systems. They consist of HV switching devices (circuit-breakers, disconnectors–earthing switches), various connecting pieces, and interface components (e.g., bushings) to overhead lines, transformers, etc. They are usually installed in the nodes of HV networks to perform switching operations needed for power system control and maintenance.

VFTs in GIS are initiated by the very fast electrical breakdown between the contacts of SF_6 disconnectors when closing or opening [1]. VFTs are electromagnetic (EM) waves traveling in the pressurized SF_6 gas volume along the GIS-components attached to the disconnector. After encountering any geometrical discontinuity (such as an insulator, open end, bushing, etc.) along their path, they are partially or totally reflected. Therefore, after being initiated as an EM impulse and continuing to exist as a superposition of a large number of different multiply reflected EM waves, VFTs have complicated nonharmonic time dependence and cover a wide frequency range from 100 kHz to 100 MHz [2].

The voltage at any particular position of the GIS section affected by VFTs is a superposition of the service voltage and VFT overvoltages (VFTOs). Therefore, the peaks of VFT voltages temporarily yield significantly higher values of voltage and electric field in GIS compared to the nominal values. As the rated voltage increases, the difference between the rated impulse withstand voltage and the VFTO decreases. For ultra high voltage (UHV) applications, VFTO can even become the dimensioning dielectric stress in certain cases.

Due to their significant influence on the GIS dielectric behavior, the VFTOs must be either accurately measured (very expensive and time consuming) or reliably predicted by simulations (cheaper and allowing for parametric studies and optimization). Up to now the predominant approach for simulating VFTOs has been based on the representation of the GIS components by their equivalent circuits with distributed parameters (transmission lines) and time-domain solution of circuit equations for the obtained equivalent network [2], [3]. The main drawback of this method is the lack of geometrical details and local field values that can be critical for the dielectric design.

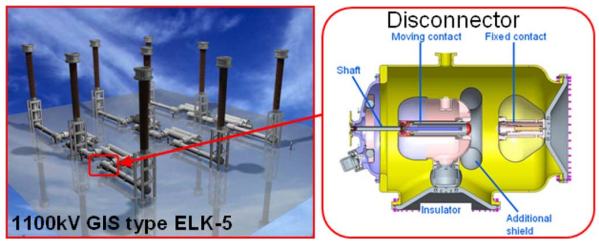

Fig. 1. 3D simplified representation of the 1100 kV GIS type ELK-5 (left), and the details of its disconnector (right) are presented.

The purpose of this paper is: 1) to suggest a new approach for simulating VFTs by directly solving Maxwell equations in time-domain on real 3D GIS geometries; 2) to present the obtained results; and 3) to perform results verification by comparison with circuit simulations and measurements on UHV GIS equipment.

The remaining part of this paper is organized as follows. The origin of the VFTs and the motivation for full-Maxwell simulations of this phenomenon are presented in Section II. Section III contains the details of our simulation algorithm and our simulation setup. The obtained numerical results are shown, analyzed, and verified in Section IV. Section V concludes this paper.

II. Origin of VFTs in GIS

The VFTs in GIS are produced by the disconnector switching operations after the electric current has already been interrupted by the attached HV circuit-breaker of the GIS. The detail of the disconnector is shown in Fig. 1 (top-right).

A typical origin of the VFTs when opening a disconnector is illustrated in Fig. 2. After the contact separation, the fixed contact, together with the attached busduct, becomes a floating potential body and the moving contact (plug), with the attached busduct, follows the electric potential (voltage) of the network, since the moving contact is attached to the network (Fig. 2, left). After the separation of the contacts, due to the finite speed of the plug, the potential difference between the contacts rises faster

Manuscript received May 31, 2010; revised July 24, 2010, October 06, 2010, and October 14, 2010; accepted October 26, 2010. Date of current version April 22, 2011. Corresponding author: J. Smajic (e-mail: jasmin.smajic@ch.abb.com).

Color versions of one or more of the figures in this paper are available online at http://ieeexplore.ieee.org.

Digital Object Identifier 10.1109/TMAG.2010.2090653

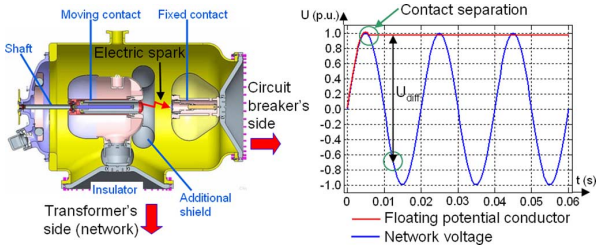

Fig. 2. The origin of the VFTs (simplified representation): The disconnector operations (left) due to the finite speed of its moving contact and rising voltage difference between its contacts $\mathrm{U_{diff}}$ (right) are accompanied by an electric breakdown between the contacts. The voltage collapse across the intercontact gap is a source of the high-frequency electromagnetic waves (VFTs) in GIS.

than the withstand voltage of the gap between the contacts (i.e., the contact distance) producing an electric breakdown between the contacts at a certain moment of time. This is shown in Fig. 2 (right), where $\mathrm{U_{diff}}$ represents the potential difference between the contacts.

The voltage collapse across the intercontact gap at restriking generates electromagnetic waves traveling in opposite directions. Being steadily reflected from the ends of the busducts, the waves superimpose and produce transient overvoltages that can be several times higher than the nominal voltage. Similarly, the VFTs are generated when closing disconnectors.

It is rather clear that the amplitude of the VFTs is directly proportional to the voltage difference between the contacts at the moment of time just before the electric restrike is ignited. According to the corresponding IEC standard [7], with higher rated voltage, the ratio *BIL voltage/rated voltage* becomes smaller (e.g., 1050 kV/245 kV ≈ 4, 2500 kV/1100 kV ≈ 2), where the abbreviation BIL stands for "Basic Insulation Level."

The classical approach to tackle this problem is to use a circuit-equations-based simulation approach implemented in EMTP-Rv commercial simulation software [6]. Namely, the GIS components can be simplified and represented as their equivalent distributed (transmission lines) or lumped (capacitance, inductance, and resistance) circuit elements. Thus, the busducts are represented as transmission lines, each local discontinuity (busduct corner, increased radius, etc.) is represented as an equivalent capacitance, the electric striking is described as a nonlinear resistor, and the attached power transformer is defined as a small network that consists of its equivalent inductance, capacitance, and resistance [2], [3]. After the equivalent circuit is assembled, the transient electric circuit equations are solved and the shape and amplitude of the VFTs are determined.

The described circuit-based simulation approach is useful to improve the overall understanding of the phenomenon and to analyze the network-GIS interaction. However, it has also the following main drawbacks: 1) smooth geometrical transitions between the components cannot be accurately modeled; 2) the lack of geometrical details and local field values that are critical for dielectric design; and 3) the insensitivity to small geometrical changes (parametric studies and optimization).

The only way to overcome the above drawbacks is to simulate the VFTs at the level of Maxwell field equations solved for 3D real-life GIS geometries. Evidently, this field-equations-based approach is very demanding from the calculation time and memory point of view. However, as it is shown in the remainder of this paper, this is now possible by using modern simulation software and computing hardware capabilities.

III. Full-Maxwell Simulations of VFTs in GIS

For full-Maxwell simulations of the VFTs the commercial field solver COMSOL was used [4]. The field formulation used for our time-domain simulations is described by the following equations [4]:

$$\nabla \times \left(\frac{1}{\mu_r}\nabla \times \vec{A}\right) + \mu_0\sigma\frac{\partial \vec{A}}{\partial t} + \mu_0\varepsilon_0\frac{\partial}{\partial t}\left(\varepsilon_r\frac{\partial \vec{A}}{\partial t}\right) = 0 \quad (1)$$

$$\vec{n} \times \vec{A} = 0 \ \text{(PEC BC)} \quad (2)$$

$$Z_{\mathrm{port}} = \frac{U_{\mathrm{port}}}{I_{\mathrm{port}}} \ \text{(Lumped port with voltage input)} \quad (3)$$

$$\vec{A}(\vec{r}, 0) = 0 \ \text{(Zero initial condition)} \quad (4)$$

where A is the magnetic vector potential, μ_0 is the magnetic permeability of vacuum, μ_r is the relative magnetic permeability, ε_0 is the electric permittivity of vacuum, ε_r is the relative electric permittivity, and Z_{port} is the wave impedance of a lumped port.

The termination of the structure and its connection with the voltage source described by (3) has, in our simulation, the following field representation [4], [5]:

$$-\vec{n} \times \left(\frac{1}{\mu_r}\nabla \times \vec{A}\right) - \frac{\mu_0}{Z_{\mathrm{PORT}}}\frac{\partial}{\partial t}\vec{n} \times (\vec{n} \times \vec{A}) = \frac{2\mu_0}{Z_{\mathrm{PORT}}}\vec{n} \times (\vec{n} \times \vec{E}_0) \quad (5)$$

where $\vec{E}_0$ is the source electric field predefined over the port's boundary.

The weak form of the boundary and initial value problem, defined by (1), (2), (4), and (5), suitable for the subsequent vector FEM discretization can be written as follows [4], [5]:

$$\begin{aligned}\int_{(\Omega)} \frac{1}{\mu_r}\nabla \times \vec{A} \cdot \nabla \times \vec{N}_i dV &+ \int_{(\Omega)} \vec{N}_i \cdot \left[\mu_0\frac{\partial}{\partial t}\left(\varepsilon_0\varepsilon_r\frac{\partial \vec{A}}{\partial t}\right) + \mu_0\sigma\frac{\partial \vec{A}}{\partial t}\right] dV + \\ &- \int_{\partial_{PORT}\Omega} \vec{N}_i \cdot \left[\frac{\mu_0}{Z_{\mathrm{PORT}}}\frac{\partial}{\partial t}\vec{n} \times (\vec{n} \times \vec{A})\right] dS \\ &= \int_{\partial_{\mathrm{PORT}}\Omega} \vec{N}_i \cdot \left[\frac{2\mu_0}{Z_{\mathrm{PORT}}}\vec{n} \times (\vec{n} \times \vec{E}_0)\right] dS \end{aligned} \quad (6)$$

where $\vec{N}_i$ is the well-known vector test function. The spatial FEM discretization of the weak form (6) was based on the linear tetrahedral vector elements [5]. This discretization process yields the following matrix equation [5]:

$$[T]\frac{\partial^2\{A\}}{\partial t^2}(t) + ([R] - [Q])\frac{\partial\{A\}}{\partial t}(t) + [S]\{A\}(t) = \{f\}(t) \quad (7)$$

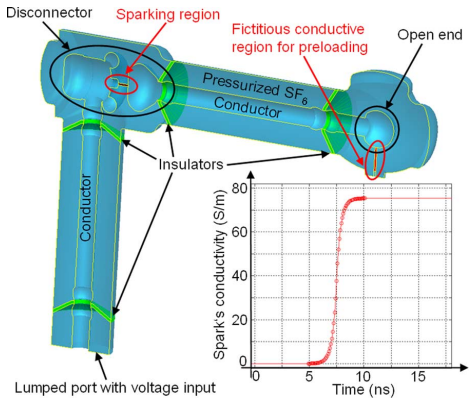

Fig. 3. The 3D simulation model of the 1100 kV GIS type ELK-5 is shown. The metal parts (enclosure, busbars, etc.) are considered to be perfect electric conductors (PEC) and, therefore, they are not included into the computational domain. This domain consists of the pressurized gas region, insulators, and striking (sparking) regions. The spark's conductivity is also presented.

where the matrix entries can be computed in the following way [5]:

$$T_{ij} = \int_{(\Omega)} \varepsilon_0 \varepsilon_r \vec{N}_i(\vec{r}) \cdot \vec{N}_j(\vec{r}) dV,$$

$$R_{ij} = \int_{(\Omega)} \sigma \vec{N}_i(\vec{r}) \cdot \vec{N}_j(\vec{r}) dV$$

$$Q_{ij} = \int_{\partial_{PORT}\Omega} \frac{1}{Z_{PORT}} \left[\vec{n} \times \vec{N}_i(\vec{r})\right] \cdot \left[\vec{n} \times \vec{N}_j(\vec{r})\right] dS$$

$$S_{ij} = \int_{(\Omega)} \frac{1}{\mu_0 \mu_r} \left[\nabla \times \vec{N}_i(\vec{r})\right] \cdot \left[\nabla \times \vec{N}_j(\vec{r})\right] dV,$$

$$f_i = \int_{\partial_{PORT}\Omega} \vec{N}_i \cdot \left[\frac{2}{Z_{PORT}} \vec{n} \times (\vec{n} \times \vec{E}_0)\right] dS. \quad (8)$$

For the time discretization of the matrix equation (7), the well known backward difference scheme (BDS) was used. The BDS scheme was chosen for its known absolute stability, i.e., its stability is not dependent on the time step [5].

The assumptions of our VFTs simulations are: 1) all conductors are considered to be perfect electric conductors (PEC); 2) the termination of the computational domain is considered to be a lumped port with voltage input; and 3) the electric strike region is considered to be low conducting with the conductivity defined according to the available experimental data.

The assumption (1) to consider metallic parts as PECs is realistic if the frequency range of the VFTs is high enough. This is justified in Section IV, where the obtained frequency range of the VFTs is presented. Considering metallic parts as PECs there is no need to mesh them since their outer surfaces are considered the boundaries of our computational domain with the boundary condition (BC) defined by (2). Thus, our computational domain consists only of the pressurized gas (SF_6 between the busducts and enclosure), insulators, and electric strike region, as shown in Fig. 3.

Assumption (2) is not very realistic as the real GIS is terminated with a bushing and power transformer connected to it. The most accurate way to model the termination of the GIS model would be to combine the field equations with electric circuit equations. Thus, the transformer and network connected to the GIS could be modeled accurately by using their equivalent circuit representations and used in our field model as a termination. This approach would be more accurate but also much more complicated and it is presently not available in the simulation tools we use. However, by using the available lumped port described by (3), we can specify the source voltage and very low wave impedance of the port to mimic the connected transformer. Since we are at the moment more interested in the transient process within the GIS than in its interaction with the network, assumption (2) is valid.

Assumption (3) is justified by the extensive experimental study that preceded our simulation activities. According to our experiments, it was possible to accurately estimate the spark's conductivity value and rise time (5 ns) based on which we have defined the function shown in Fig. 3.

The electric sparking model used in our simulations is a very simple conductivity function presented in Fig. 3. The moment of time when the electric spark is ignited is chosen prior to the start of the simulation.

The spark is not conductive at the beginning of our time-domain simulations and electrodes are charged to certain different potentials that are determined based on the worst possible scenario principle, as described in the disconnector switching type test duties 1 and 2 [7]. After the loading process is complete, the spark conductivity is changing according to the function shown in Fig. 3. The rise time T_{rise} is rather short ($5 \cdot 10^{-9}$ s) and the corresponding voltage collapse between the disconnector's contacts generates the high-frequency waves that propagate back and forth within the GIS.

It is worth mentioning that the spark conductivity definition is very important for the stability of the time-domain simulations. As one can see in Fig. 3, the spark conductivity is modeled by using smooth exponential functions and in the regions of the conductivity's abrupt change a large number of sampling points are defined. Such a smooth function, together with a carefully chosen time-step in simulations, will ensure the numerical stability.

It is also important to mention that the electric spark model is very far from reality. To accurately describe an electric spark one has to couple the electromagnetic theory, radiation theory, and fluid flow theory, i.e., one must solve the so-called magneto-hydro-dynamic (MHD) equations which are beyond the purpose of our simulations and beyond the scope of this paper. Since we are more interested in propagation of the electromagnetic waves produced by the spark than in the sparking process itself this simplified electric spark model is accurate enough.

IV. Numerical Results

The VFT results were obtained by performing time-domain full-Maxwell simulations. The obtained results can be compiled into an animation that reveals the real nature of the VFTs. Several interesting frames of such an animation are shown in Fig. 4. The first frame (top-left) shows the electric field at the moment of time just before the electric spark is ignited. As one can see the most intensive electric field is established between the disconnector's contacts as they are charged to opposite voltages. The next two frames (top-right and bottom-left) represent the traveling electromagnetic waves at two different moments of

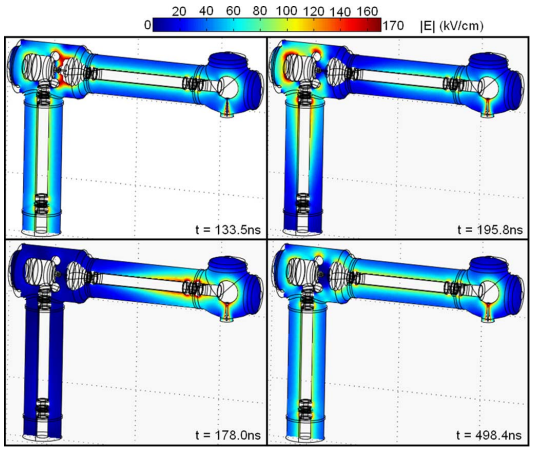

Fig. 4. The results of the 3D time-domain full-Maxwell simulations of the 1100 kV GIS type ELK-5 are shown. The absolute value of the electric field is depicted. The charged electrodes (top-left) before the arc is ignited, the traveling waves (top-right and bottom-left), and the steady state after the VFTs were partially dissipated and partially guided out of the GIS (bottom-right) are presented.

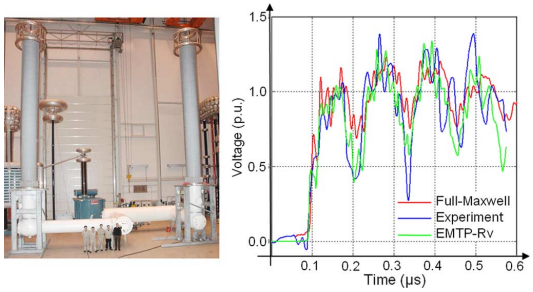

Fig. 5. The test setup (left) for VFTO testing of ELK-5 and comparison of the numerical results (right) is presented. The results of the full-Maxwell simulations, EMTP-Rv electric circuit equations, and measurements are compared. More details can be found in the text.

time after the spark ignition. The last frame shows the steady state after the VFTs are partially dissipated (the spark has a finite resistance of around 3 Ω) and partially guided out through the lumped port.

To follow the VFTs testing procedure of ELK-5 presented in Fig. 5 (left), the bushing was added into our simulation model. The obtained results were compared against the circuit-equations-based EMTP-Rv results and against measurements.

This comparison is shown in Fig. 5 (right). The voltage peak reached the value of 1500 kV which is 35% higher than the rated voltage. Evidently, major wave reflections are accurately computed since the number and timing of the dominant voltage peaks and dips correspond well to the experiment. The average relative disagreement between the field simulation and experiment was 18.84%, which is acceptable, considering the geometrical complexity of the 3D real-life model, physical complexity of the phenomenon itself, and anticipated measurement precision. The average error of the EMTP-Rv results was 15.66% which is slightly better than the accuracy of the field simulations. The reason for this is that the EMTP-Rv model takes into account the connected power transformer and network. However, the full-Maxwell simulations are much richer in details inside the GIS which is of paramount importance for improving design. Specifically, the voltage and field stress over the conductor surfaces and shields of GIS components are obtained by these simulations.

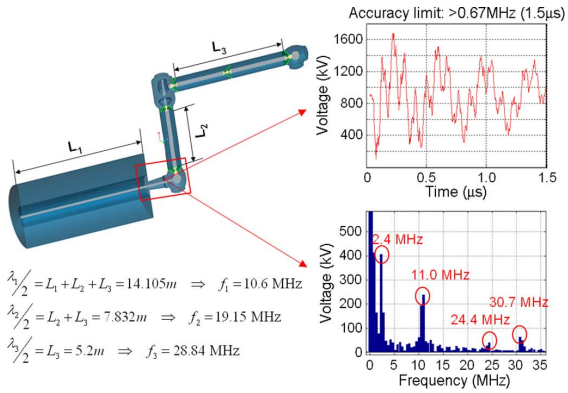

Fig. 6. The results of the 3D time-domain full-Maxwell simulations of the 890 kV GIS type ELK-4 are shown. The voltage across the first GIS insulator was computed and the fast Fourier transformation of the signal was performed. The frequency spectrum of the VFTs is shown. Evidently, the dominant harmonic components correspond well to the lengths of the main GIS sections. More details can be found in the text.

The results of the VFTs computation for the 890 kV GIS type ELK-4 presented in Fig. 6 reveal the VFTs frequency range. The voltage across the insulator closest to the GIS disconnector was recorded over time, the fast Fourier transformation of the signal was performed, and the harmonic components of the signal were obtained. As shown in Fig. 6, the most dominant harmonic components of the VFTOs match very well with the lengths of the main GIS sections.

The results presented in Figs. 5 and 6 are obtained by solving the FEM models with around 2 million elements each. To solve such a model on a modern multicore machine (Intel Xeon 2.5 GHz, 32 GB RAM) takes around 15 h.

V. Conclusion

The algorithm for 3D full-Maxwell simulation of VFTs in GIS is presented and the obtained results are analyzed and verified by comparison against measurements and circuit-equations-based simulations. The shape of the dominant electromagnetic waves in GIS was accurately predicated. The average disagreement between the obtained results and measurements of 18.84% is acceptable for the purpose of improving design.

Acknowledgment

The authors would like to acknowledge their gratitude to U. Kruesi and D. Sologuren-Sanchez of ABB Switzerland Ltd. for interesting discussions and valuable suggestions during the simulation work presented in this paper.

References

[1] J. Meppelnik, K. Diederich, K. Feser, and W. Pfaff, "Very fast transients in GIS," *IEEE Trans. Power Delivery*, vol. 4, no. 1, pp. 223–233, Jan. 1989.
[2] D. Povh, H. Schmitt, O. Völcker, and R. Witzmann, "Modelling and analysis guidelines for very fast transients," *IEEE Trans. Power Delivery*, vol. 11, no. 4, pp. 2028–2035, Oct. 1996.
[3] "Guidelines for representation of network elements when calculating transients," Working Group 02 of Study Committee 33, Paris, France, CIGRE Rep., 2000.
[4] COMSOL Multiphysics. [Online]. Available: www.comsol.com
[5] J. Jin, *The Finite Element Method in Electromagnetics*, 2nd ed. New York: Wiley, 2002.
[6] EMTP RV, EM Transient Program. [Online]. Available: http://www.emtp.com
[7] *High-Voltage Switchgear and Controlgear*, IEC 62271-203, International Electrotechnical Comission, Geneva, Switzerland, 2003.